

Chapter 1

Future Gravitational Wave Detectors Based on Atom Interferometry

Remi Geiger

*LNE-SYRTE, Observatoire de Paris, PSL Research University,
CNRS, Sorbonne Universités, UPMC Univ.*

Paris 06, 61 avenue de l'Observatoire, 75014 Paris, France.

Contents

1. Introduction	2
2. Detector based on two distant light-pulse atom interferometers	4
2.1. Principle of the light-pulse atom interferometer	4
2.2. Atom interferometer phase shift in the presence of a GW	6
2.3. Gradiometer configuration.	10
2.4. Quantum limited strain sensitivity curve	11
3. Experimental techniques	13
4. Main noise sources and mitigation strategies	15
4.1. Strategies for the rejection of laser frequency noise	16
4.2. Rejection of the gravity gradient noise with an array of atom interferometers	17
4.3. Comparison with other GW detectors	19
4.4. Other noise sources	20
5. Current projects and perspectives	20
5.1. The Matter-wave laser Interferometric Gravitation Antenna (MIGA) project	21
5.2. Challenges	23
6. Conclusion	23
7. Acknowledgements	25
References	25

Abstract: *We present the perspective of using atom interferometry for gravitational wave (GW) detection in the mHz to about 10 Hz frequency band. We focus on light-pulse atom interferometers which have been subject to intense developments in the last 25 years. We calculate the effect of the GW on the atom interferometer and present in details the atomic gradiometer configuration which has retained more attention recently. The principle of such a detector is to use free falling atoms to measure the phase of a laser, which is modified by the GW. We highlight the potential benefits of using atom interferometry compared to optical interferometry as well as the challenges which remain for the realization of an atom interferometry based GW detector. We present some of the important noise sources which are expected in such detectors and strategies to circumvent them. Experimental techniques related to cold atom interferometers are briefly explained. We finally present the current progress and projects in this rapidly evolving field.*

1. Introduction

Matter-wave interferometry relies on the wave nature of massive particles to realize an interferometer, in analogy with optical interferometry which exploits the wave nature of photons [1]. Several illustrations of matter-wave interference phenomena have been demonstrated in the 20th century including interference with electron Cooper pairs [2], neutrons [3], atoms [4] or molecules [5]. Atom interferometry has benefited from the important progress in the field of cold atom physics which started in the 1980's. The first proofs of principle of atom interferometers (AIs) in 1991 [4, 6–9] triggered significant experimental developments. In particular, the possibility to extend the Ramsey sequence with optical fields to build an atom interferometer based on the atomic recoil triggered many experiments [10]. The experimental developments led to the realization of different types of AIs addressing several applications, such as inertial sensing [11, 12], precision measurements of fundamental constants [13, 14], fundamental physics [15, 16], and gravimetry [17, 18].

Parallel to the emergence of concepts for gravitational wave (GW) detectors based on laser interferometry, studies were conducted on the effect of gravitational fields in matter-wave interferometry in the 1970s [19, 20], and later in laser spectroscopy [21]. Less than 10 years after the pioneering experiments of 1991, the field of atom interferometry had already been subject to an important progress, for example with the demonstration of a sensitive atomic gravimeter [22] and gyroscope [23], and owing to the rapid development of cold atom physics. Such progress motivated reconsidering

the application to GW detection.

To this end, various theoretical frameworks were proposed, such as a generalization of the Klein-Gordon equation [24], a generalization of the Dirac equation in curved space-time [5], or a generalization of the ABCD matrix formalism of optics to matter-wave propagation [25]. In 2004, Chiao and Speliotopoulos publish a paper where they analyze the sensitivity of a matter-wave interferometer using atomic beams emanating from a supersonic atomic source, and claim favorable sensitivities for such devices compared to space-based GW detectors based on laser interferometry [26]. Their paper is however subject to debate [27, 28], the various authors finding different results because they studied different physical experiments. As analyzed in [29], the important aspect of such studies lies in the interpretation of the coordinate systems and of the boundary conditions in order to obtain the same result for various descriptions of the experiment, which is at the basis of general relativity.

Rapidly, several teams start to work on the estimation of the sensitivity of AIs for GW detection. Delva *et al* [30], and Tino and Vetrano (following the work of Bordé) [31] find the same result for the GW induced phase shift in an AI :

$$\Delta\phi \sim h_{\text{GW}}L/\lambda_{\text{dB}}, \quad (1)$$

where h_{GW} is the strain amplitude of the GW and L is the physical separation between the two arms of the interferometer. The signal is inversely proportional to the de Broglie wavelength of the atom of mass m , $\lambda_{\text{dB}} \sim h/mv_L$, with v_L being the velocity of the atoms entering the interferometer and h the Planck constant. If we consider the case of a light-pulse AI, where the splitting of the atomic wave is performed on a light standing wave (2.1 will present this AI in details), then the physical separation between the two interferometer arms is given by $L = T\hbar k/m$, with $k = 2\pi/\lambda_{\text{laser}}$ the optical wavevector of the light grating, T the time spent by the atoms in the interferometer region and $\hbar = h/2\pi$. Eq. (1) then simplifies in

$$\Delta\phi \sim h_{\text{GW}} \frac{Tv_L}{\lambda_{\text{laser}}}, \quad (2)$$

illustrating that it is favorable to use beams of fast atoms and rather long devices (to increase the interrogation time T).

The authors discuss the comparison with optical interferometers where the phase shift can be written in a similar form as Eq. (1) [30]. The interpretation is then the following: the AI can potentially be more sensitive

than the optical interferometer for the same linear dimension and level of phase noise, because the wavelength of the wave is much shorter for atomic waves ($\lambda_{\text{dB}} \sim \text{pm}$ for beams at few 100 m.s^{-1}) than for optical waves ($\lambda_{\text{light}} \sim \text{hundreds of nm}$). However, the AI cannot compete with optical interferometers for two reasons: (i) it is very difficult to realize an interferometer with arm separations L exceeding the meter scale (compared to kilometer scale optical ones); (ii) the flux \dot{n} which determines the detection noise of the interferometer given by $\sigma_\phi \sim 1/\sqrt{\dot{n}}$ is more than 10 orders of magnitude smaller for atomic sources than for photons in a laser. Besides these considerations, these papers do not analyze the other noise sources which could limit the sensitivity of the detector.

The strategy for detecting GWs with AIs evolves with a paper of 2008 [32]. In this article, the authors formalize the idea of using the AI to read the phase of a laser which is modified by the GW, in analogy with the mirrors which are used as phase references in optical GW detectors. To reject the position noise which degrades the sensitivity of laser interferometers, they propose a gradiometer configuration with two distant AIs interrogated by the same laser beam. It is this idea of the gradiometer configuration which has then retained much attention and which we will describe in details in this chapter.

2. Detector based on two distant light-pulse atom interferometers

2.1. Principle of the light-pulse atom interferometer

We start the description of a GW detector based on atom interferometry by describing the origin of the phase shift in a light-pulse AI, where the atomic waves are diffracted on a light grating. The diffraction process is represented in Fig. 1. Various schemes exist to realize this diffraction, such as two photon Raman transitions [7] or Bragg diffraction [33]. In both schemes, the atom absorbs a photon from one beam (momentum $\hbar k_1$) and stimulatedly emit a photon from the other beam (momentum $\hbar k_2$). If the two beams are counterpropagating, the momentum of the atom changes by $\hbar(k_1 + k_2) \equiv \hbar k_{\text{eff}}$ which is about twice the optical wavenumber of the electromagnetic fields used in the process ($k_{\text{eff}} \simeq 2k_1$). Such two photon transition enables to create quantum superpositions of two momentum states $|\vec{p}\rangle$ and $|\vec{p} + \hbar\vec{k}_{\text{eff}}\rangle$ of the atom, which represent the 2 arms of the interferometer. For optical transitions in atoms, the typical momentum transfer is of the order

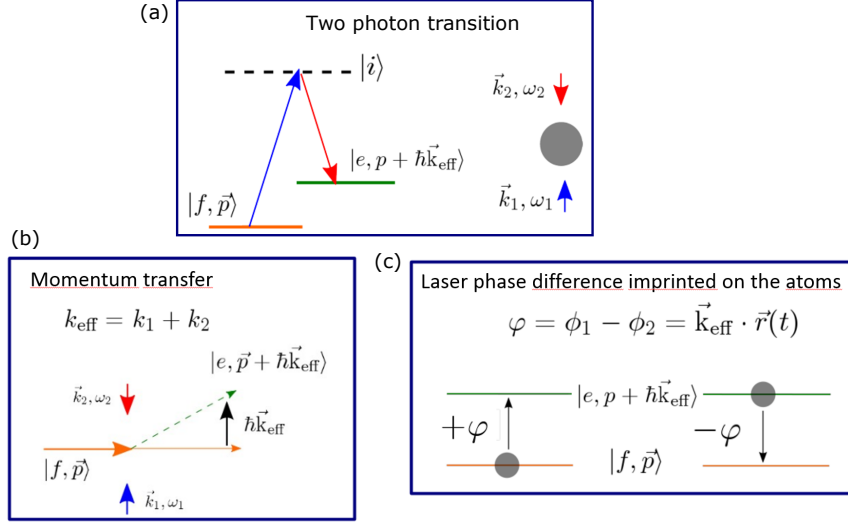


Fig. 1. (a) Stimulated two photon transition coupling two momentum states in a 3-level atom. (b) The two-photon transition enables to create quantum superpositions of the two momentum states and thus to create two arms in an interferometer. (c) During the diffraction process, the relative phase $\varphi = \phi_1 - \phi_2$ between the two lasers is imprinted on the diffracted part of the atomic wavefunction.

of 1 cm/s. Besides the physical separation, the relative phase $\varphi = \phi_1 - \phi_2$ between the two lasers is imprinted on the diffracted part of the atomic wavefunction [34].

In analogy with the optical Mach-Zehnder interferometer, it is possible to realize an AI consisting of three light pulses which respectively split, redirect and recombine the atomic wave (see Fig. 2). The three light pulses thus act similarly as the beam splitters and mirrors in an optical interferometer. The beam splitter or mirror condition can be obtained by varying the interaction strength of the laser-atom interaction (e.g. by varying the light pulse duration). The phase difference between the two arms can be computed from the relative laser phases imprinted at the different times on the atom and reads $\Delta\phi = \varphi(0) - 2\varphi(T) + \varphi(2T)$, with T the time between the light pulses [34]. As an illustration, in the case where the AI is used as a gravimeter, the light beams propagate parallel to the local gravity acceleration and the AI phase is given by $\Delta\phi = \vec{k}_{\text{eff}} \cdot \vec{g}T^2$. This allows to perform absolute measurements of the gravity acceleration at the 10^{-9} relative precision level [17, 18, 22].

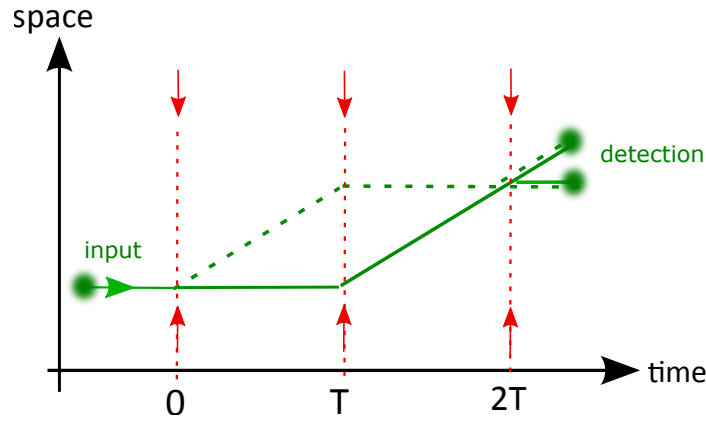


Fig. 2. Space-time diagram of the light-pulse atom interferometer (AI). The red arrows represent the two counterpropagating lasers and the green lines represent the path of the atomic waves.

2.2. Atom interferometer phase shift in the presence of a GW

We present here a derivation of the light-pulse AI phase shift in the presence of a GW. We will concentrate on the effect of the GW on the phase of the lasers, which is imprinted on the atomic wavepacket at the diffraction events. We will not consider the effect of the GW on the phase of the atomic waves themselves (see Eq. (1)), as it is negligible compared to the laser induced phase in the configuration which will be considered. We refer, e.g., to Ref. [35] [Eq. (24)] for the full expression with both the laser induced phase and the AI phase contributions. We will come back to this approximation in the conclusion 6.

The scheme of the laser interrogation is shown in Fig. 3, where the laser beam is retroreflected. We remind that the phase difference between the two arms in the AI essentially originates from the local phase of the lasers which is imprinted onto the diffracted wave-packet at the interaction points [34, 36]. Therefore, the calculation of the AI phase reduces to the calculation of the laser phase of the two counterpropagating beams. We will use the Einstein Coordinates to describe the experiment, where the GW affects the propagation of light and the atoms are freely falling, i.e. used as phase discriminators. The same result is obtained when considering a different coordinate system [35, 36].

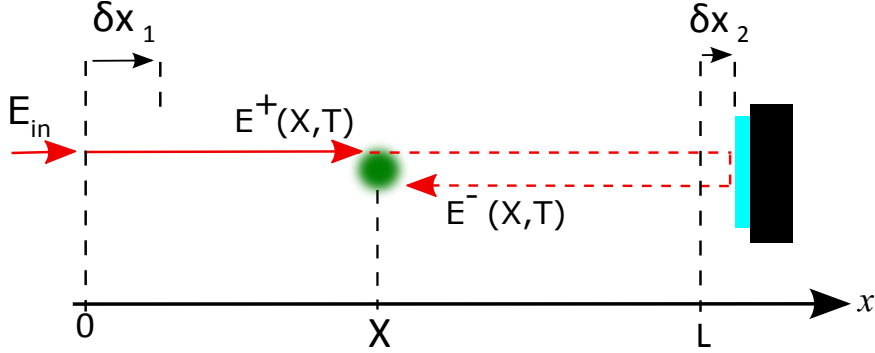


Fig. 3. Laser interrogation scheme and notations used in the calculation of the AI phase shifts. $\delta x_1(t)$ and $\delta x_2(t)$ are the position fluctuations of the input optics and of the retroreflecting mirror with respect to the fixed baseline L , respectively.

(a) calculation of the phase of the lasers. We decompose the electromagnetic field as a superposition of two counterpropagating waves, $E^\pm(t)$, respectively propagating towards positive and negative x (see Fig. 3). The AI phase shift is determined by the *relative* phase between $E^+(t)$ and $E^-(t)$, which is imprinted on the atoms at position X . We will determine this relative phase as a function of the mirror position, the frequency of the laser, and the gravitational wave (GW) amplitude.

We consider the effect of a GW propagating in the direction perpendicular to the plane of Fig. 3 and polarized along the laser propagation direction (x). We describe the propagation of electromagnetic (EM) waves in the x direction. The relativistic invariant is given by [37]:

$$ds^2 = c^2 dt^2 - dx^2 + h(t) dx^2 = 0, \quad (3)$$

where $h(t)$ is the amplitude of the GW. For weak GW, the solution is

$$dx = \pm [1 + \frac{1}{2} h(t)] c dt, \quad (4)$$

where the plus (minus) sign corresponds to the light propagating from left to right (right to left). The EM wave is emitted at time t^+ from the left input optics (position $\delta x_1(t^+)$) and arrives at time T at the position X , where it interacts with the atoms. The emission time t^+ is given by:

$$\int_{\delta x_1(t^+)}^X dx = c[T - t^+] + \frac{c}{2} \int_{t^+}^T h(t) dt. \quad (5)$$

Using perturbation theory with $t^+ \approx T - X/c$, we obtain at first order in $\delta x_1, h$:

$$t^+ \approx T - \frac{X - \delta x_1(T - \frac{X}{c})}{c} + \frac{1}{2} \int_{T - \frac{X}{c}}^T h(t) dt. \quad (6)$$

In a similar way, we obtain the emission time t^- of the EM wave which propagates to the right mirror, is reflected, and propagates back in opposite direction to arrive at position X at time T , where it interacts with the atoms. Taking into account the propagation from the right mirror to the atoms, t^- is given by:

$$t^- = T - \frac{1}{c} \left[2L - X + 2\delta x_2 \left(T - \frac{L - X}{c} \right) - \delta x_1 \left(T - \frac{2L - X}{c} \right) \right] + \frac{1}{2} \int_{T - \frac{2L - X}{c}}^T h(t) dt. \quad (7)$$

At the space-time event (X, T) , the atoms interact with two counterpropagating fields $E^\pm(X, T)$, which we define by

$$E^\pm(X, T) \equiv E(t^\pm). \quad (8)$$

The relative phase $\Delta\varphi = \varphi^+ - \varphi^-$ imprinted on the atoms during the atom diffraction is thus determined by the time delay $t^+ - t^-$ between the two emission events, which is obtained from Eqs. (6) and (7).

We now consider only slow fluctuations of $\delta x_i(t)$ and $h(t)$ corresponding to frequencies $\omega/2\pi \ll (2L/c)^{-1}$. In particular, we neglect the position fluctuations on a time-scale smaller than the light round-trip time from the atoms to the retroreflecting mirror. This condition can be ensured by the use of a dedicated suspension system of the optics (see Chapter ??)]. In this approximation the fluctuations in Eqs. (6) and (7) are evaluated at time T and become:

$$t^+ \approx T - \frac{X}{c} + \frac{\delta x_1(T)}{c} + \frac{X}{2c} h(T) \quad (9)$$

$$t^- \approx t^+ - \frac{2(L - X)}{c} - \frac{2\delta x_2(T)}{c} + \frac{2(L - X)}{2c} h(T). \quad (10)$$

To account for laser phase noise, we write the EM field as

$$E(t) = E_{in}(t) e^{i\alpha(t)} \quad (11)$$

where $E_{in}(t)$ is the amplitude of the EM field just after the input optics and

$$\alpha(t) = 2\pi\nu_0 t + \tilde{\phi}(t) \quad (12)$$

is the laser phase. Here ν_0 is the injection laser frequency and $\tilde{\phi}(t)$ is the laser phase noise. Assuming that the phase noise is small and slowly varying, we express it as

$$\tilde{\phi}(t + \Delta t) \approx \phi_0 + 2\pi\delta\nu(t)\Delta t, \quad (13)$$

where $\delta\nu(t)$ is the frequency noise of the laser. This approximation is valid as long as Δt is smaller than the typical inverse bandwidth of the noise, meaning that in a sufficiently small region of time around t , the phase is proportional to the instantaneous frequency ($\nu_0 + \delta\nu(t)$) of the laser field.

With this model for the phase noise, we obtain the following expression for the EM field at the point of interaction with the atoms:

$$E^+(X, T) \equiv E(t^+) = E_{in}(t^+)e^{i\alpha(t^+)}, \quad (14)$$

with

$$\alpha(t^+) \approx 2\pi\nu_0 t^+ + \phi_0 + 2\pi\delta\nu(T)(t^+ - T). \quad (15)$$

Using the above equation for t^+ , we thus obtain:

$$E^+(X, T) \approx E_{in}(T)e^{2i\pi T[\nu_0 + \delta\nu(T)] + i\phi_0} e^{i\varphi^+(X, T)} \quad (16)$$

with

$$\varphi^+(X, T) = -\frac{2\pi\nu_0}{c}X + \frac{2\pi\nu_0}{c}\delta x_1(T) + \frac{2\pi}{c}[-\delta\nu(T) + \frac{\nu_0}{2}h(T)]X. \quad (17)$$

From now on, we will omit the time argument (T) in the variables $\{\delta x_i, \delta\nu, h\}$ for clarity of the equations. A similar calculation for the E^- field yields the phase

$$\varphi^-(X) = -\frac{2\pi\nu_0}{c}(2L - X) + \frac{2\pi\nu_0}{c}[\delta x_1 - 2\delta x_2] + \frac{2\pi}{c}[-\delta\nu + \frac{\nu_0}{2}h](2L - X). \quad (18)$$

The relative phase $\Delta\varphi = \varphi^+ - \varphi^-$ imprinted on the atoms during the diffraction is thus:

$$\Delta\varphi(X) = 2k \left[(L - X) + \delta x_2 + \left[\frac{\delta\nu}{\nu_0} - \frac{h}{2} \right] (L - X) \right], \quad (19)$$

where $k = 2\pi\nu_0/c$ is the laser wavevector. In the retroreflecting configuration, the position noise δx_1 of the input optics is common to both beam and is therefore not present in Eq. (19).

(b) Sensitivity function of the atom interferometer. The AI phase is determined by the relative phase of the EM fields given by Eq. (19), and by the sensitivity function $s(t)$ of the three light-pulse AI. The formalism of the sensitivity function was introduced in the context of atomic clocks to describe the response of an atom interferometer to fluctuating phase contributions (the Fourier transform of $s(t)$ corresponds to the transfer function of the AI). A description of the formalism as well as a measurement of the sensitivity function can be found in [38].

Besides the sensitivity function, AIs operate sequentially and deliver a measurement every cycle of duration $T_c = T_{\text{prep}} + 2T + T_{\text{det}}$ during which the atoms are prepared (e.g. laser cooled during a period T_{prep}), interrogated in the AI (duration $2T$) and detected at the AI output (duration T_{det}). The AI output signal at cycle m is then given by the convolution product

$$s_\varphi(X, mT_c) = \Delta\varphi(X, t) \otimes s(t - mT_c), \quad (20)$$

with $s(t) \approx \delta(t - 2T) - 2\delta(t - T) + \delta(t)$ and $\delta(t)$ the Dirac distribution. For simplification, we neglected in this expression of the sensitivity function the finite duration of the light pulse (the full expression can be found in [38]). This approximation corresponds to neglecting the phase fluctuations (e.g. due to $\{\delta x_i(t), \delta\nu(t), h(t)\}$) of frequencies higher than the Rabi frequency of the two-photon transition, which typically lies in the tens of kHz range.

(c) Full expression of the AI phase. Using Eqs. (20) and (19), the output signal of the AI at cycle m reads

$$s_\varphi(X, mT_c) = 2k \left[-\delta x(X, t) + \delta x_2(t) + \left(\frac{\delta\nu(t)}{\nu_0} - \frac{h(t)}{2} \right) (L - X) \right] \otimes s(t - mT_c). \quad (21)$$

Here, $\delta x(X, t)$ represents the motion of the atoms along the laser beam direction due to the fluctuations of the local gravitational acceleration. This contribution corresponds to the first term $2k(L - X)$ appearing in Eq. (19) which we rewrote as follows for more clarity: *(i)* as L is a constant, it does not contribute to the AI signal and disappears; *(ii)* to highlight the fact that X might fluctuate because of temporal variations of the local gravitational field in the x direction, we change for the notation $\delta x(X, t)$. We will focus on this contribution in the section on gravity gradient noise reduction 4.2.

2.3. Gradiometer configuration.

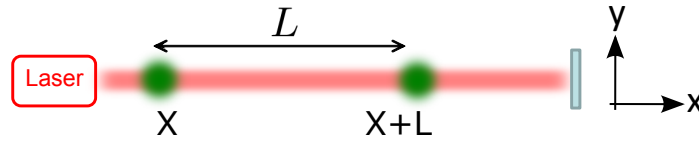


Fig. 4. Gradiometer configuration: two distant AIs (green clouds) are interrogated by the same laser beam.

We now consider the gradiometer configuration sketched in Fig. 4. Taking the differential signal $\psi(X, mT_c) = s_\varphi(X, mT_c) - s_\varphi(X + L, mT_c)$ be-

tween two AIs separated by the distance L yields:

$$\psi(X, mT_c) = 2k \left[L \left(\frac{\ddot{h}(t)}{2} - \frac{\delta\ddot{\nu}(t)}{\nu_0} \right) + \delta X(X+L, t) - \delta X(X, t) \right] \otimes s(t-mT_c). \quad (22)$$

This equation can be rewritten in terms of the local gravity acceleration as

$$\psi(X, mT_c) = 2k \left[L \left(\frac{\ddot{h}(t)}{2} - \frac{\delta\ddot{\nu}(t)}{\nu_0} \right) + a_x(X+L, t) - a_x(X, t) \right] \otimes s_\alpha(t-mT_c) \quad (23)$$

where $a_x(X, t) = \partial_t^2[\delta x(X, t)]$ is the local gravity acceleration in the x direction and $s_\alpha(t)$ is the AI sensitivity function to acceleration, given by $\ddot{s}_\alpha(t) = s(t)$.

The very important aspect in this equation is that the position noise $\delta x_2(t)$ of the retroreflecting mirror has been rejected by the gradiometer configuration. To be more precise, position fluctuations of frequencies smaller than $(2L/c)^{-1}$ are rejected, which represents the major part of the position noise in optical GW detectors (see Chapter ??). Rejection of the vibration noise in gradiometer configuration has already been measured in AIs (rejection by 140 dB was demonstrated in [39]). This important immunity to position noise of the AI gradiometer makes such instruments good candidates for GW detectors operating at lower frequencies than ground based optical interferometers, which sensitivity are limited at frequencies below ~ 10 Hz by position noise of the optics (vibration noise, thermal noise, etc) (see Chapter ??).

Eq. (23) also shows that fluctuations of the local gravity field result in an acceleration signal $a_x(X, t)$ whose gradient will have the same signature as that of the GW. Therefore, it is impossible to distinguish the effect of a GW from that of a fluctuating gravity gradient. This fundamental limitation is known as the gravity gradient noise limit, or Newtonian Noise limit, and has been the subject of several studies in ground-based optical GW detectors [40]. We will explore the possibility to reduce the Newtonian Noise with AIs in section 4.2.

2.4. Quantum limited strain sensitivity curve

To illustrate the potential performance of the AI detector, we will assume in this paragraph that the detector is limited by the quantum noise, i.e. we neglect in particular the contribution of laser frequency noise and Newtonian noise which appear in Eq. (23). The power spectral density (PSD) of

the gradiometer output is then given by

$$S_\psi(\omega) = (2nkL)^2 \omega^4 \frac{S_h(\omega)}{4} |\hat{s}_\alpha(\omega)|^2 + 2S_\phi(\omega), \quad (24)$$

where S_h is the PSD of the GW, S_ϕ is the PSD of the AI phase noise (the factor 2 accounts for the 2 AIs involved in the gradiometer), and $\hat{s}_\alpha(\omega) = \text{FT}[s_\alpha(t)] = 4 \sin^2(\omega T/2) / \omega^2$ is the Fourier transform of the AI sensitivity function to acceleration.

The factor n in Eq. (26) denotes the number of momenta transferred to the atom during the diffraction process, which amplifies the phase signal by a factor of n . It is analogous to the use of Fabry-Perot cavities which amplify the phase signal in laser interferometers. Such process called large momentum transfer (LMT) beam splitters is now frequently used in AI experiments to enhance the sensitivity of the interferometer (see, e.g. [41, 42]). Proof of principle AIs with $n = 100$ have been reported.

The phase noise PSD for an AI limited by quantum noise can be written as

$$S_\phi(\omega) = \frac{\eta}{\dot{N}_{at}} \left(\frac{\text{rad}^2}{\text{Hz}} \right) \quad (25)$$

where \dot{N}_{at} is the cold atom flux (in s^{-1}) and $\eta \leq 1$ is a factor which accounts for a possible measurement noise reduction with respect to the standard quantum limit ($\eta \approx 0.01$ has been reported in [43]).

If we consider a minimum sensitivity with a signal to noise ratio of 1, we obtain the strain sensitivity function:

$$(S_h(\omega))^{1/2} = \left(\frac{2\eta}{\dot{N}_{at}} \right)^{1/2} \frac{1}{4Lnk \sin^2(\omega T/2)}. \quad (26)$$

We plot in Fig. 5 the strain sensitivity function for various parameters of the AI gradiometer. The blue line corresponds to an optimized AI combining several state of the art techniques, i.e. with a phase noise of $10^{-6} \frac{\text{rad}^2}{\text{Hz}}$ and a 20 photon LMT beam splitter ($n = 10$), and a gradiometer baseline $L = 1$ km. The red curve corresponds to the much more ambitious scenario which could be obtained in the future with $10^{-14} \frac{\text{rad}^2}{\text{Hz}}$ phase noise, $n = 1000$ and $L = 10$ km. In both cases, we considered an interrogation time $2T = 0.6$ s, which determines the frequency $f_0 = 1/2T$ corresponding to the best sensitivity. Such interrogation time is typical and would allow to cover the frequency band $\sim 0.1 - 10$ Hz. Using longer interrogation times T does not change the value of the peak sensitivity but shifts the operating bandwidth to lower frequencies. Long (> 10 s) interrogation times in AIs using ultracold

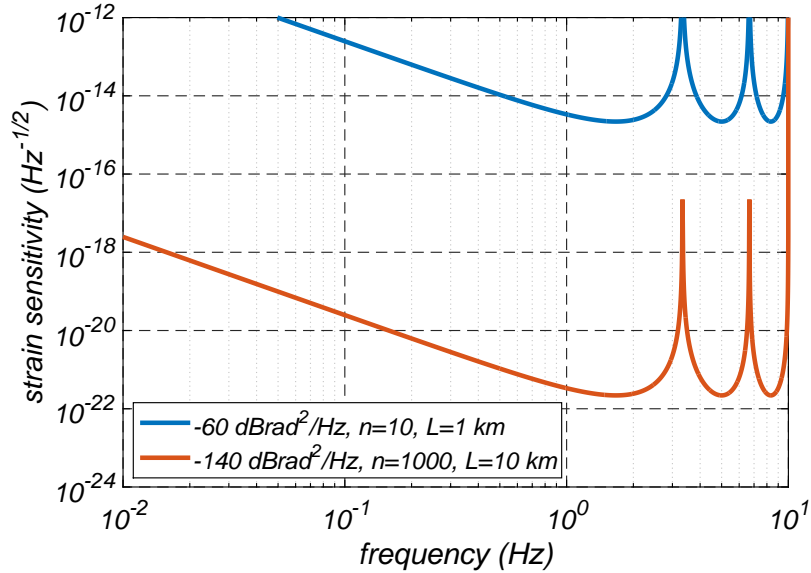


Fig. 5. Quantum limited strain sensitivity curve of the AI gradiometer GW detector for different parameters of the AI. In both cases $T = 0.3$ s.

atoms (temperature < 10 nK) could then be used to design space-based detectors operating in the mHz regime [32]. Finally, we neglected here the sequential operation of the AI, i.e. we neglected the possible aliasing effects due to the finite sampling period T_c of the AI. We will discuss this approximation in the context of increasing the AI bandwidth at the end of the chapter, section 5.2.

3. Experimental techniques

In this section, we briefly present the main experimental techniques for realizing a cold atom interferometer. Various type of AIs exist; we present here the architecture which has led to the most significant results in the field, and which is currently mostly considered for applications to GW detection.

Why cold atoms ? Cold atoms are necessary to realize the light-pulse AI sensitive to inertial effects presented in section 2.1. The requirement on the atom temperature comes from the interrogation time of the atoms

in the interferometer, in the range of hundreds of milliseconds. For an atom cloud with rms velocity σ_v , its radius after a time $2T$ of free propagation is $\sigma_r \simeq 2\sigma_v T$, which must be kept smaller than the interrogation laser beam radius. For a 1 cm waist laser beam, this condition places a bound on the rms velocity in the cm/s regime, corresponding to μK temperatures (depending on the mass of the atom). Besides such transverse selection (atoms escaping transversely from the laser beam), the frequency of the laser is Doppler shifted depending on the atom velocities. If the Doppler width $k_{\text{eff}}\sigma_v$ of the distribution is greater than the Rabi frequency $\Omega/2\pi$ of the two-photon transition, then some atoms will not undergo the transition, which will reduce the contrast of the AI. For typical laser powers corresponding to $\Omega/2\pi \sim 50$ kHz, the velocity selection condition also requires atom temperatures in the μK regime.

Experimental sequence. The typical experimental sequence is sketched in Fig. 6. It starts by laser cooling the atoms in an ultra-high vacuum chamber (pressure $\sim 10^{-10}$ mBar) (a). A detailed and pedagogical description of the associated physics and experimental techniques is presented in [44]. Alkaline atoms have first been preferred because of their relatively simple electronic structure and of available laser sources. For example, Rubidium 87 has extensively been used in cold atom experiments, because of the availability of laser sources at 780 nm to cool this atom and manipulate its quantum states with electric dipole transitions. The laser cooling step lasts typically hundreds of milliseconds to one second and produces $10^8 - 10^9$ atoms at a temperature close to $1 \mu K$ in a volume of few mm^3 . The atom source is then further prepared before entering the AI region, in order to improve its coherence (b) and (c): this includes, for example, a selection of the atoms in the $m_F = 0$ Zeeman sublevel which is less sensitive to magnetic fields, and a velocity selection light pulse to enter the interferometer with a narrow (few 100 nK) longitudinal velocity distribution (in the direction of the AI lasers). As a result, about $10^6 - 10^7$ useful atoms participate to the interferometer (d). At the AI output, the population of atoms in each port is measured, for example by fluorescence detection with photodiodes (e). This allows to reconstruct the probability of transition of the atom from the AI input state to one of the output states (f). This transition probability is modulated by the AI phase (g).

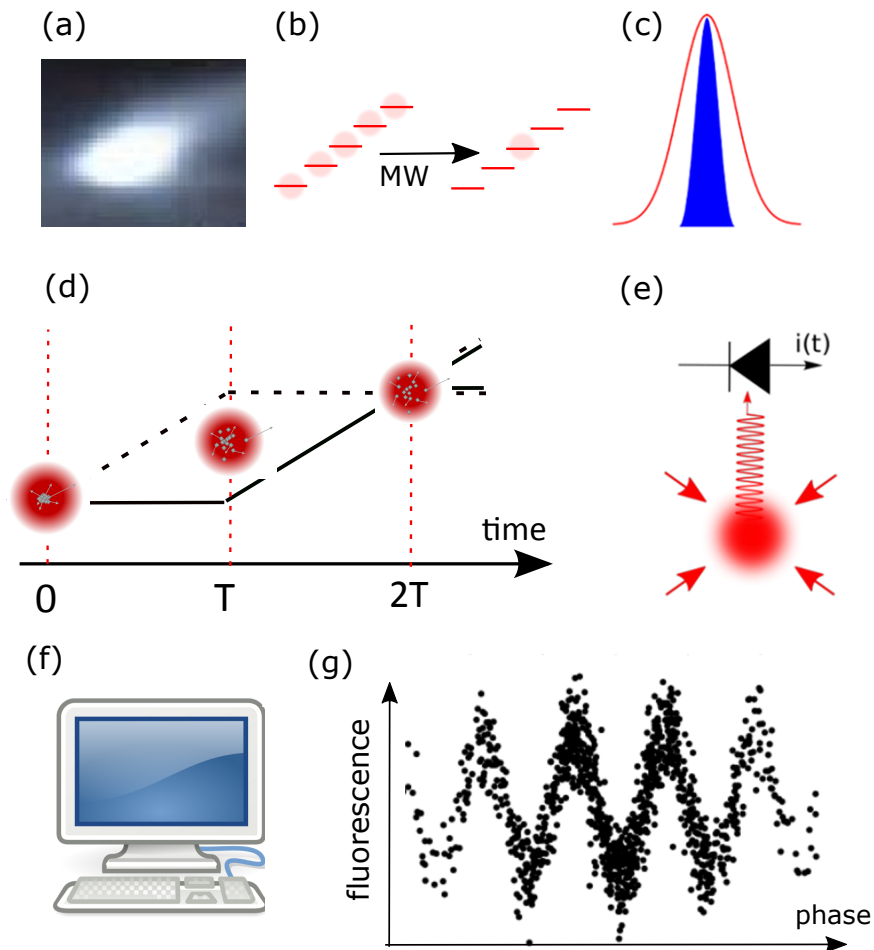


Fig. 6. Typical AI experimental sequence. (a) Laser cooling of the atoms in a Magneto-Optical-Trap. (b) Selection of the $m_F = 0$ Zeeman sublevel. (c) Longitudinal velocity selection (only the blue distribution will participate to the AI). (d) Light-pulse AI sequence. (e) Fluorescence detection of the AI output atoms. (f) Data analysis. (g) Interference fringes where each point correspond to one experimental cycle.

4. Main noise sources and mitigation strategies

As was shown at the end of section 2.2, position noise of the optics is mainly rejected in the AI gradiometer configuration, which represents an important advantage of atom interferometry compared to laser interferometry.

However, several other noise sources will affect a detector based on AIs. We review in this section some of the main noise sources. We focus on two important noise sources which are common to laser and atom interferometry: laser frequency noise and Newtonian noise. We present the strategies which were proposed to reduce these noise sources in detectors based on AI.

4.1. *Strategies for the rejection of laser frequency noise*

As shown in Eq. 23, the effect of the GW is indistinguishable from a fluctuation of the interrogation laser frequency at the same frequency: this is encoded in the term $L(h/2 + \delta\nu/\nu)$. The origin of the sensitivity to laser frequency noise comes from the propagation delay between the two counter-propagating lasers originating from different locations. In the retroreflecting configuration which we considered (Fig. 3), the extra phase accumulated by the beam which travels to the mirror and reflects back to the atoms is $2k(L - X_1)$ (see Eq. (17)), yielding a fluctuation $2\delta k(L - X_1)$ if the laser frequency fluctuates by $\delta k = 2\pi\delta\nu/c$. For the other AI situated at a different location X_2 with respect to the retroreflecting mirror, the effect of the laser noise is different. Therefore, in the gradiometer configuration, the effect of laser noise amounts $2\delta k(X_2 - X_1)$. The influence of laser frequency noise in such light-pulse AIs has been measured in [45]. Aiming at strain sensitivities of $10^{-20}/\sqrt{\text{Hz}}$ or lower in the frequency band $\sim 0.1 - 10$ Hz requires a laser with a relative frequency stability better than this level, or dedicated strategies for laser noise rejection/reduction.

Multiple arm configuration. A first possibility to reduce the effect of laser frequency noise is to adopt a cross arm configuration [32, 46, 47], as in laser Michelson interferometric GW detectors. Considering a symmetric configuration consisting of 2 orthogonal arms of same length and interrogated by the same laser, laser frequency noise is rejected for a GW with (+) polarization. In laser interferometers, the degree of asymmetry between the 2 arms sets the rejection efficiency for laser noise, which is typically 99% (see Chapter ??) and limited by the asymmetry between the optical modes resonating in the two cavities. To achieve the required stability, the laser is therefore stabilized on the common mode of the Michelson interferometer, i.e. on the ultrastable km-long cavities inside the interferometer arm. This allows to reach a relative frequency stability $\sim 10^{-21}/\sqrt{\text{Hz}}$ in the detector frequency band, thus a strain sensitivity $\sim 0.01 \times 10^{-21}/\sqrt{\text{Hz}}$. The rejection

of laser frequency noise in a cross arm detector using AIs has been discussed briefly in Ref. [47], but the rejection efficiency in various geometries has not been analyzed in enough details yet.

Single laser AIs. In 2011, Yu and Tinto propose an AI detector configuration based on a single laser operating two distant AIs, instead of the two lasers considered so far [48]. Their proposal exploits coherent superpositions of two atomic levels separated by an energy corresponding to an optical transition, as in optical clocks. In such a scheme, the momentum transfer is performed by a single transition between two levels, instead of a two-photon transition involving 3 levels as in the case of Fig. 1 which we considered so far. Atoms characterized by a long (\sim second) lifetime of the optically excited state can be used for such a protocol, as it is the case for example for alkaline-Earth-like atoms used in optical clocks (Calcium, Strontium, Ytterbium). As only one laser is used to drive the transition, the problem explained above of laser noise sensitivity due to the propagation delay in a *single* AI disappears. Another interpretation is to say that the AI compares the phase of the laser against the atomic internal clock coherence [48].

Yu and Tinto conclude their article by considerations on the sensitivity of their proposed detector, and highlight the need to use large momentum transfer techniques (LMT, obtained by multiphoton transitions) to enhance the sensitivity of the detector. Their idea is extended for the LMT configuration and further detailed in [49] in the context of a space-based detector. The authors claim favorable sensitivities at milli-Hertz frequencies compared to space-based laser interferometers such as LISA. The complexity of such a mission is discussed in [50], in particular the need for very large laser powers required to drive the highly forbidden optical transition between the two (optical) clock state. To conclude this paragraph, we note that a Strontium AI using LMT beam splitter has been reported in 2015 [51], and that many developments of AI with ultracold alkaline-Earth-like atoms are currently carried out by several research groups. We can expect a promising future for this technology.

4.2. Rejection of the gravity gradient noise with an array of atom interferometers

As shown by Eq. 23, the effect of the GW cannot be distinguished from that of a fluctuating gravity gradient by using two AIs. This problem is

similar to optical GW detectors which use two test masses (the two cavity mirrors of one interferometer arm) to probe the effect of the GW. This fundamental limit for GW detectors operating on Earth is known as the Newtonian Noise (NN) limit. For ground based detectors, it represents a fundamental limit which prevents from observing GW at frequencies below few Hz, because the NN starts to dominate at these frequencies [40, 52].

NN originates from mass fluctuations in the surrounding of the detector, which translate in gravity field fluctuations at the test masses. Sources of NN are, for example, seismic noise triggering stochastic fluctuations of the ground density and resulting in fluctuations of the gravity field (so called seismic NN), or air density fluctuations in the atmosphere caused by turbulence (so called infrasound NN).

An article published in 2016 presents a method to go beyond the NN limit in GW detectors based on atom interferometry [47]. The method relies on the fact that the spatial properties of the NN are different than the spatial properties of the GW: while the wavelength c/f of the GW at $f = 1$ Hz is 3×10^8 m, the characteristic length $v/2f$ of the NN at such frequency is of order 1 km [40] (v is the velocity of seismic waves for the seismic NN, or of the sound in air for infrasound NN). Therefore, by operating an array of spatially distributed AIs interrogated by the same laser beam, it is possible to average the NN to zero. This idea is sketched in Fig. 7.

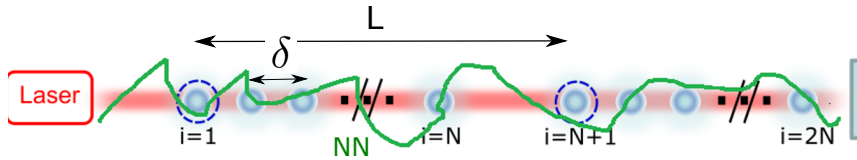


Fig. 7. Principle of the rejection of the Newtonian Noise (NN) with an array of spatially distributed AIs. L is the gradiometer baseline and δ is the spatial sampling period.

More precisely, the detector consists of N gradiometers of baseline L , and which sample the NN with a spatial step δ . The average signal

$$H_N(t) = \frac{1}{N} \sum_{i=1}^N \psi(t, X_i), \quad (27)$$

with the $\psi(X)$ signal given by Eq. (23). This procedure yields the GW signal and a residue of the NN which standard deviation is reduced by \sqrt{N} compared to the single gradiometer case, if the N measurements are

uncorrelated. Using the spatial behavior of the NN correlation function, the authors show that a rejection of the NN greater than \sqrt{N} can be obtained. For a scenario with $N = 80$, it is shown that rejection efficiencies of up to 30 can be achieved at 1 Hz.

4.3. Comparison with other GW detectors

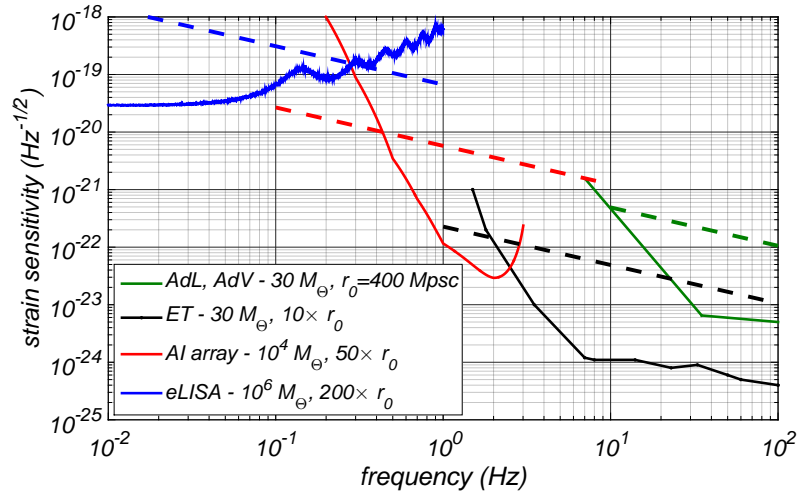


Fig. 8. Strain sensitivity curves of current and possible future GW detectors (plain lines). Dashed lines indicate the required sensitivity to detect the GW from a compact binary following Eq. (28); M_{\odot} is the mass of the sun and $r_0 = 400 \text{ Mpc}$. We assumed a detection with a signal to noise ratio of 1. AdV: Advanced VIRGO [53], AdL: Advanced LIGO [54]; ET (Einstein Telescope) is a ground-based laser interferometer proposal [55]. eLISA [56] is a space-based laser interferometer proposal. The AI array is a ground-based AI proposal [47].

The window opened by the AI array proposition described in the previous section would enable to cover a frequency band where no other detector is currently planned to operate, as shown in Fig. 8. The parameters of the AI detector (red line) are those of Ref. [47]: a phase noise level of $10^{-7} \text{ rad}/\sqrt{\text{Hz}}$, LMT beam splitters with $n = 1000$ and a detector baseline $L = 16 \text{ km}$. The quantum noise is moreover reduced by a factor \sqrt{N} thanks to the array of N AI. In Fig. 8, we show strain sensitivity functions for different detectors (plain lines) and simple estimates for the GW signal (dashed lines) corresponding to compact binaries as sources of the GW.

We parametrized the binaries by the mass of the stars and their luminosity distance, and assumed a detection with signal to noise ratio of 1. To obtain the estimate of the signal strength for the compact binary, we followed the simple model of [46] [Eq.(11) to (18)] yielding

$$\sqrt{[S_h(\omega)]} \simeq 0.3 \times \eta^{1/2} c^{-3/2} f^{-2/3} (GM)^{5/6} r^{-1} \quad (28)$$

with $\eta = m_1 m_2 / M^2$ the symmetric mass ratio ($M = m_1 + m_2$), f the GW frequency and r the luminosity distance. We refer to Ref. [57] and chapter ?? for more details on the sources.

4.4. Other noise sources

Several noise sources already identified in atom interferometry experiments will potentially affect the sensitivity of the GW detector. While the gradiometer configuration gives immunity to some of the noise sources because they are common to both AIs, several other backgrounds might affect the sensitivity and will depend on the exact nature of the detector, e.g. two-photon transitions or single photon transitions to realize the diffraction. Some of them have been analyzed in [32, 58] for the 2-photon transition case which we focused on in this chapter, and in [49, 50] for the single photon case. To cite few, we can mention the effect of wavefront distortions of the laser beam which might be seen differently by the two distant AIs, magnetic field fluctuations, effects of rotations on the interferometer, residual effect of vibrations or laser phase noise.

5. Current projects and perspectives

While several research groups worldwide are developing new atom interferometry techniques, and studying theoretically the application to GW detection, only few teams started to realize an instrument which could address this application. High sensitivity AIs using LMT techniques, ultracold atoms and long interrogation times in tall vacuum chambers are being constructed in USA [59], China [60], Australia [61] and Europe [62]. However, hybrid laser-atom interferometers based on the gradiometer configuration, which is primarily considered for application to GW detection, require long baseline instruments. We present here the only project which, to date and to our knowledge, is being pursued towards the application to GW detection with a long (> 100 m) instrument: the Matter-wave laser Interferometric Gravitation Antenna (MIGA) project currently under construction in Europe.

5.1. The Matter-wave laser Interferometric Gravitation Antenna (MIGA) project

The MIGA project started in 2013 with an initial funding from the French nation research agency (ANR), and involves about 15 institutes with expertise in atomic physics, metrology, gravitational physics and geosciences. The goal of the project is to design and realize an instrument capable of serving as a demonstrator for a future GW antenna based on atom interferometry. The instrument will also be used for precision gravity field measurements, with important applications in geosciences, in particular hydrology [63]. The initial idea of the instrument is based on the gradiometer configuration described in section 2, with a baseline $L = 300$ m, and the possibility to correlate several AIs interrogated by the same laser beam. Details on the design and realization of the subsystems of MIGA can be found in [58, 63, 64]. We briefly describe here the main elements of the instrument, which commissioning should start in 2018.

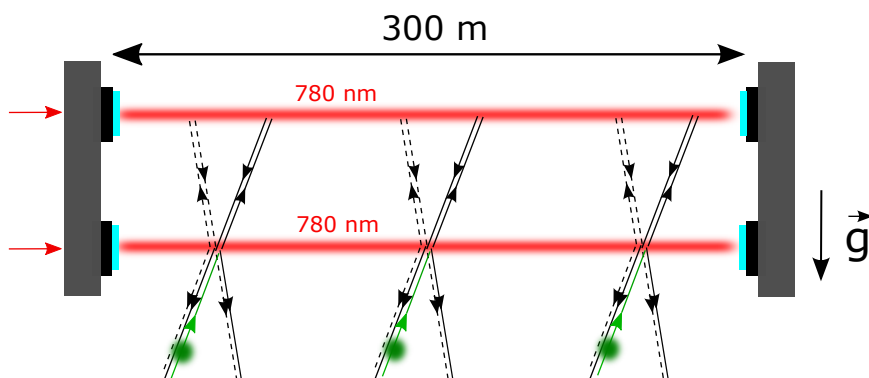


Fig. 9. Geometry of the MIGA instrument (not to scale, the separation between the two AI arms being of order of few cm). The atoms are launched from below from the magneto-optical trap (not shown). Bragg diffraction on lasers resonating in an optical cavity is used as matter-wave optics, which requires to enter the AI with the correct angle. The Bragg angle (\sim mrad) is exaggerated here for clarity. The interrogation time is $2T = 500$ ms for a 3 light-pulse AI with apogee of the atom trajectory at the top beam.

Fig. 9 shows the geometry of the MIGA instrument where the optical mode of two optical cavities interrogate simultaneously 3 AIs separated by a distance of about 150 m. The optical cavity will allow to enhance the optical power at the cavity resonance by the optical gain ($\simeq 10$ in the initial design) in order to improve the efficiency of LMT beam splitters which require large

laser powers. The length of the cavity will be stabilized using a 1560 nm wavelength laser stabilized at the 10^{-15} relative frequency stability. The AIs use Bragg diffraction of ^{87}Rb on the light standing wave in the cavity (wavelength 780 nm), where momentum states $| - n\hbar k \rangle$ and $| + n\hbar k \rangle$ are coupled by the (high order) Bragg diffraction. LMT beam splitters with $n \simeq 5$ are initially planned for atom sources with temperature in the μK range. In this figure, the cold atom source is not shown. Atoms are cooled in a magneto-optical trap (MOT) located about 1 meter below the first Bragg beam, and launched vertically at a velocity close to 5 m/s. On its way up, the atom source is prepared as mentioned in section 3. After the AI, on the way down, the atomic state is probed by fluorescence detection, which allows to measure the interferometer phase shift.

The instrument will be installed at the low noise underground laboratory LSBB located in the South-East of France [65], see Fig. 10. Two 300 meter galleries will be dug dedicatedly for the detector. Besides the vacuum tube, the optical systems and the AI sensors, various environmental instruments will be deployed in order to monitor the environment around the detector and assess applications in hydrology: superconducting gravimeters, seismometers, radars or muon detectors.

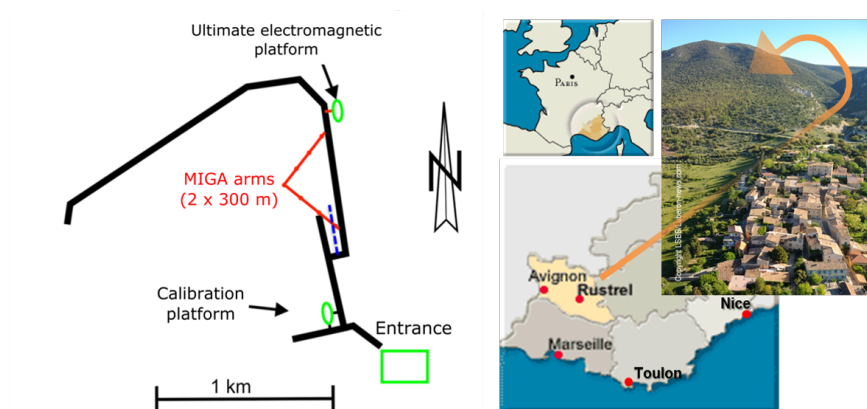


Fig. 10. Installation site of the MIGA instrument at the low noise underground laboratory in the South-East of France.

While the MIGA instrument has not been designed for GW detection applications because of its relatively small (300 m) baseline and the lack of maturity of cold atom technology at the start of the project, it will serve as a first demonstrator for a future larger detector, at the European or inter-

national scale. Among the first tests which will be performed, correlations between distant AI sensors in an optical cavity, gravity gradient measurements at the $10^{-13} \text{ s}^{-2}/\sqrt{\text{Hz}}$ level, and validation of the state of the art AI technology in a large detector will have an important impact on the design of a future instrument.

5.2. Challenges

As shown in section 2.4, reaching strain sensitivities of order $10^{-22}/\sqrt{\text{Hz}}$ in the $\sim 0.1 - 10 \text{ Hz}$ frequency band will require many technology developments. The technology should progress by about 10 orders of magnitude in strain sensitivity to be fully useful for GW astronomy. Many of the required techniques have been demonstrated independently in various experiments. Given the rapid progress in the field in the last 20 years, we can thus expect breakthroughs in the next decades. On the basis of the detector design presented in this chapter, future instruments will probably require

- (1) LMT beam splitting techniques [41, 42, 66, 67];
- (2) ultracold atoms [68, 69];
- (3) quantum enhanced phase measurements [43] and/or much brighter cold atom sources [70–72]
- (4) higher sampling rates/continuous operation of the AI [73, 74].

The challenge will consist in realizing an instrument which combines all these techniques. The table below summarizes the requirements, as well as the state of the art. A new concept of detector based on different ideas than that presented here would allow to revisit these numbers and require less ambitious values.

We conclude this section by comparing the signal of the AI gradiometer Ψ_{gradio} to that associated with the effect of the GW on a single AI, $\Delta\phi$, given by eq. (2). The ratio between the two contributions is

$$\frac{\Psi_{\text{gradio}}}{\Delta\phi} \sim \frac{Lnk}{Tv_Lnk} = \frac{L}{v_LT} \approx \frac{10^4 \text{ m}}{10 \text{ m.s}^{-1} \times 1 \text{ s}} = 10^3, \quad (29)$$

It shows that the contribution from the differential laser phase imprinted on the AI dominates over the GW induced phase on the atomic wave in a single AI. This estimation should however be revisited in details.

6. Conclusion

GW astronomy will benefit from the largest frequency band covered by different detectors. While the performance of current ground based laser

Table 1. Technology requirements for a GW detector based on a AI gradiometer configuration to reach a strain sensitivity of $10^{-22}/\sqrt{\text{Hz}}$. The "current" column corresponds to demonstrated results in different experiments. The "required" column implies that all techniques are operational in the same experiment.

AI parameter	current	required
LMT order (n)	100	1000
temperature ^a	1 nK	?
interrogation time T (s)	0.1 – 1	~ 0.3
AI operating frequency (Hz)	5	20
phase sensitivity (dBrad/ $\sqrt{\text{Hz}}$)	-30	-70
detector baseline	300 m	> 3 km
strain sensitivity ($/\sqrt{\text{Hz}}$)	10^{-10}	10^{-22}

^aLow

temperatures are required for high contrast AIs based on LMT diffraction, but this requirement depends on the available power of the laser which drives the LMT pulse.

interferometers is impressive and triggered GW astronomy, their sensitivity at frequencies below 10 Hz might strongly be limited. It is therefore important to look for complementary solutions. One possible solution is to use cold atoms as test masses to probe the phase of the laser influenced by the GW. Such solutions started to be studied in the 2000' after the rapid progress of the field of atom interferometry. This is the possibility which has been described in this chapter.

GW detectors based on AI rely on probing the phase of a laser with free falling cold atoms, and are characterized by an important immunity to position noise of the optics. Moreover, strategies have been proposed to reduce some of the noise sources identified in laser interferometric detectors, such as laser frequency noise or gravity gradient noise. In this chapter, we presented strategies for designing a ground based GW detector sensitive in the $\sim 0.1 - 10$ Hz frequency band. Besides the principle of a detector based on atom interferometry, we presented the current projects which have started to design of a future GW detector, as well as the many technological challenges that remain.

The schemes which were initially studied and abandoned because of experimental complexity should be reconsidered, taking into account the important technological progress in the field of atomic physics. In particular the possibility to use a single AI based on relativistic particles for GW detection should be revisited.

7. Acknowledgements

I would like to thank my collaborators from the atom interferometry and inertial sensor team of the SYRTE laboratory and from the MIGA consortium. I thank Pacôme Delva and Christian Bordé for their useful comments on the historical aspects of the introduction.

References

- [1] P. Berman, *Atom Interferometry*. Elsevier Science (1997). ISBN 9780080527680. URL <https://books.google.fr/books?id=D0fDPFAcaMkC>.
- [2] J. E. Zimmerman and J. E. Mercereau, Compton wavelength of superconducting electrons, *Phys. Rev. Lett.* **14**(22), 887–888 (May, 1965). doi: 10.1103/PhysRevLett.14.887.
- [3] H. Rauch, W. Treimer, and U. Bonse, Test of a single crystal neutron interferometer, *Physics Letters A.* **47**(5), 369 – 371 (1974). ISSN 0375-9601. doi: DOI:10.1016/0375-9601(74)90132-7. URL <http://www.sciencedirect.com/science/article/pii/0375960174901327>.
- [4] D. W. Keith, C. R. Ekstrom, Q. A. Turchette, and D. E. Pritchard, An interferometer for atoms, *Phys. Rev. Lett.* **66**(21), 2693–2696 (May, 1991). doi: 10.1103/PhysRevLett.66.2693.
- [5] C. Bordé, N. Courtier, F. du Burck, A. Goncharov, and M. Gorlicki, Molecular interferometry experiments, *Physics Letters A.* **188**(3), 187–197 (May, 1994). ISSN 0375-9601. URL <http://www.sciencedirect.com/science/article/pii/0375960194904375>.
- [6] F. Riehle, T. Kisters, A. Witte, J. Helmcke, and C. J. Bordé, Optical ramsay spectroscopy in a rotating frame: Sagnac effect in a matter-wave interferometer, *Phys. Rev. Lett.* **67**(2), 177–180 (Jul, 1991). doi: 10.1103/PhysRevLett.67.177.
- [7] M. Kasevich and S. Chu, Atomic interferometry using stimulated raman transitions, *Phys. Rev. Lett.* **67**, 181–184 (Jul, 1991). doi: 10.1103/PhysRevLett.67.181. URL <http://link.aps.org/doi/10.1103/PhysRevLett.67.181>.
- [8] O. Carnal and J. Mlynek, Young’s double-slit experiment with atoms: A simple atom interferometer, *Phys. Rev. Lett.* **66**, 2689–2692 (May, 1991). doi: 10.1103/PhysRevLett.66.2689. URL <http://link.aps.org/doi/10.1103/PhysRevLett.66.2689>.
- [9] J. Robert, C. Miniatura, S. L. Boiteux, J. Reinhardt, V. Bocvarski, and J. Baudon, Atomic interferometry with metastable hydrogen atoms, *EPL (Europhysics Letters)*. **16**(1), 29– (1991). ISSN 0295-5075. URL <http://stacks.iop.org/0295-5075/16/i=1/a=006>.
- [10] C. Bordé, Atomic interferometry with internal state labelling, *Physics Letters A.* **140**(1), 10–12 (1989). ISSN 0375-9601. URL <http://www.sciencedirect.com/science/article/pii/0375960189905379>.
- [11] B. Canuel, F. Leduc, D. Holleville, A. Gauguier, J. Fils, A. Virdis, A. Clairon,

- N. Dimarcq, C. J. Bordé, A. Landragin, and P. Bouyer, Six-axis inertial sensor using cold-atom interferometry, *Phys. Rev. Lett.* **97**, 010402 (Jul, 2006). doi: 10.1103/PhysRevLett.97.010402. URL <http://link.aps.org/doi/10.1103/PhysRevLett.97.010402>.
- [12] R. Geiger, V. Menoret, G. Stern, N. Zahzam, P. Cheinet, B. Battelier, A. Villing, F. Moron, M. Lours, Y. Bidel, A. Bresson, A. Landragin, and P. Bouyer, Detecting inertial effects with airborne matter-wave interferometry, *Nat Commun.* **2**, 474– (Sept., 2011). URL <http://dx.doi.org/10.1038/ncomms1479>.
- [13] R. Bouchendira, P. Cladé, S. Guellati-Khélifa, F. Nez, and F. Biraben, New determination of the fine structure constant and test of the quantum electrodynamics, *Phys. Rev. Lett.* **106**, 080801 (Feb, 2011). doi: 10.1103/PhysRevLett.106.080801. URL <http://link.aps.org/doi/10.1103/PhysRevLett.106.080801>.
- [14] G. Rosi, F. Sorrentino, L. Cacciapuoti, M. Prevedelli, and G. M. Tino, Precision measurement of the newtonian gravitational constant using cold atoms, *Nature.* **510**(7506), 518–521 (June, 2014). ISSN 0028-0836. URL <http://dx.doi.org/10.1038/nature13433>.
- [15] S. Lepoutre, A. Gauguier, G. Tréner, M. Büchner, and J. Vigué, He-mckellar-wilkens topological phase in atom interferometry, *Phys. Rev. Lett.* **109**, 120404 (Sep, 2012). doi: 10.1103/PhysRevLett.109.120404. URL <http://link.aps.org/doi/10.1103/PhysRevLett.109.120404>.
- [16] L. Zhou, S. Long, B. Tang, X. Chen, F. Gao, W. Peng, W. Duan, J. Zhong, Z. Xiong, J. Wang, Y. Zhang, and M. Zhan, Test of equivalence principle at 10^{-8} level by a dual-species double-diffraction raman atom interferometer, *Phys. Rev. Lett.* **115**, 013004 (Jul, 2015). doi: 10.1103/PhysRevLett.115.013004. URL <http://link.aps.org/doi/10.1103/PhysRevLett.115.013004>.
- [17] P. Gillot, O. Francis, A. Landragin, F. P. D. Santos, and S. Merlet, Stability comparison of two absolute gravimeters: optical versus atomic interferometers, *Metrologia.* **51**(5), L15 (2014). URL <http://stacks.iop.org/0026-1394/51/i=5/a=L15>.
- [18] C. Freier, M. Hauth, V. Schkolnik, B. Leykauf, M. Schilling, H. Wziontek, H.-G. Scherneck, J. Müller, and A. Peters. Mobile quantum gravity sensor with unprecedented stability. (2015).
- [19] B. Linet and P. Tourrenc, Changement de phase dans un champ de gravitation: Possibilité de détection interférentielle, *Can. J. Phys.* **54**(11), 1129–1133 (June, 1976). ISSN 0008-4204. doi: 10.1139/p76-136. URL <http://dx.doi.org/10.1139/p76-136>.
- [20] L. Stodolsky, Matter and light wave interferometry in gravitational fields, *General Relativity and Gravitation.* **11**(6), 391–405 (1979). ISSN 1572-9532. doi: 10.1007/BF00759302. URL <http://dx.doi.org/10.1007/BF00759302>.
- [21] C. J. Bordé, J. Sharma, P. Tourrenc, and T. Damour, Theoretical approaches to laser spectroscopy in the presence of gravitational fields, *J. Physique Lett.* **44**(24), 983–990 (1983). URL <http://dx.doi.org/10.1051/jphyslet:019830044024098300>.

- [22] A. Peters, K. Y. Chung, and S. Chu, High-precision gravity measurements using atom interferometry, *Metrologia*. **38**(1), 25– (2001). ISSN 0026-1394. URL <http://stacks.iop.org/0026-1394/38/i=1/a=4>.
- [23] T. L. Gustavson, A. Landragin, and M. A. Kasevich, Rotation sensing with a dual atom-interferometer sagnac gyroscope, *Classical and Quantum Gravity*. **17**(12), 2385– (2000). ISSN 0264-9381. URL <http://stacks.iop.org/0264-9381/17/i=12/a=311>.
- [24] Y. Q. Cai and G. Papini, Particle interferometry in weak gravitational fields, *Classical and Quantum Gravity*. **6**(3), 407 (1989). URL <http://stacks.iop.org/0264-9381/6/i=3/a=017>.
- [25] C. J. Bordé, Theoretical tools for atom optics and interferometry, *C. R. Acad. Sci. Paris*. **t. 2, sÈrie IV**, 509–530 (2001).
- [26] R. Y. Chiao and A. D. Speliotopoulos, Towards migo, the matter-wave interferometric gravitational-wave observatory, and the intersection of quantum mechanics with general relativity, *Journal of Modern Optics*. **51**(6-7), 861–899 (Apr., 2004). ISSN 0950-0340. doi: 10.1080/09500340408233603. URL <http://www.tandfonline.com/doi/abs/10.1080/09500340408233603>.
- [27] S. Foffa, A. Gasparini, M. Papucci, and R. Sturani, Sensitivity of a small matter-wave interferometer to gravitational waves, *Phys. Rev. D*. **73**, 022001 (Jan, 2006). doi: 10.1103/PhysRevD.73.022001. URL <http://link.aps.org/doi/10.1103/PhysRevD.73.022001>.
- [28] A. Roura, D. R. Brill, B. L. Hu, C. W. Misner, and W. D. Phillips, Gravitational wave detectors based on matter wave interferometers (migo) are no better than laser interferometers (ligo), *Phys. Rev. D*. **73**, 084018 (Apr, 2006). doi: 10.1103/PhysRevD.73.084018. URL <http://link.aps.org/doi/10.1103/PhysRevD.73.084018>.
- [29] P. Delva, M.-C. Angonin, and P. Tournenc, Matter waves and the detection of gravitational waves, *Journal of Physics: Conference Series*. **66**(1), 012050– (2007). ISSN 1742-6596. URL <http://stacks.iop.org/1742-6596/66/i=1/a=012050>.
- [30] P. Delva, M.-C. Angonin, and P. Tournenc, A comparison between matter wave and light wave interferometers for the detection of gravitational waves, *Physics Letters A*. **357**(4Ài5), 249–254 (Sept., 2006). ISSN 0375-9601. URL <http://www.sciencedirect.com/science/article/pii/S0375960106006335>.
- [31] G. M. Tino and F. Vetrano, Is it possible to detect gravitational waves with atom interferometers?, *Classical and Quantum Gravity*. **24**(9), 2167– (2007). ISSN 0264-9381. URL <http://stacks.iop.org/0264-9381/24/i=9/a=001>.
- [32] S. Dimopoulos, P. W. Graham, J. M. Hogan, M. A. Kasevich, and S. Rajendran, Atomic gravitational wave interferometric sensor, *Phys. Rev. D*. **78**, 122002 (Dec, 2008). doi: 10.1103/PhysRevD.78.122002.
- [33] D. M. Giltner, R. W. McGowan, and S. A. Lee, Theoretical and experimental study of the bragg scattering of atoms from a standing light wave, *Phys. Rev. A*. **52**, 3966–3972 (Nov, 1995). doi: 10.1103/PhysRevA.52.3966.
- [34] P. Storey and C. Cohen-Tannoudji, The feynman path integral approach to atomic interferometry, *J. Phys. II France*. **4**, 1999 (1994).

- [35] G. Tino and F. Vetrano, Atom interferometers for gravitational wave detection: a look at a ???simple??? configuration, *General Relativity and Gravitation*. **43**(7), 2037–2051 (2011). ISSN 0001-7701.
- [36] C. Bordé, Quantum theory of atom-wave beam splitters and application to multidimensional atomic gravito-inertial sensors, *General Relativity and Gravitation*. **36**(3), 475–502 (2004). ISSN 0001-7701.
- [37] J.-Y. Vinet (2016). The VIRGO physics book, Chapter 2: Optics and related topics, available at <http://www.virgo-gw.eu/vpb/>.
- [38] P. Cheinet, B. Canuel, F. Pereira Dos Santos, A. Gauguier, F. Leduc, and A. Landragin, Measurement of the sensitivity function in time-domain atomic interferometer, *IEEE Trans. on Instrum. Meas.* **57**, 1141 (2008).
- [39] J. M. McGuirk, G. T. Foster, J. B. Fixler, M. J. Snadden, and M. A. Kasevich, Sensitive absolute-gravity gradiometry using atom interferometry, *Phys. Rev. A*. **65**, 033608 (Feb, 2002). doi: 10.1103/PhysRevA.65.033608. URL <http://link.aps.org/doi/10.1103/PhysRevA.65.033608>.
- [40] P. R. Saulson, Terrestrial gravitational noise on a gravitational wave antenna, *Phys. Rev. D*. **30**, 732–736 (Aug, 1984). doi: 10.1103/PhysRevD.30.732. URL <http://link.aps.org/doi/10.1103/PhysRevD.30.732>.
- [41] P. Cladé, S. Guellati-Khélifa, F. Nez, and F. Biraben, Large momentum beam splitter using bloch oscillations, *Phys. Rev. Lett.* **102**, 240402 (Jun, 2009). doi: 10.1103/PhysRevLett.102.240402. URL <http://link.aps.org/doi/10.1103/PhysRevLett.102.240402>.
- [42] S.-w. Chiow, T. Kovachy, H.-C. Chien, and M. A. Kasevich, 102 hk large area atom interferometers, *Phys. Rev. Lett.* **107**, 130403 (Sep, 2011).
- [43] O. Hosten, N. J. Engelsen, R. Krishnakumar, and M. A. Kasevich, Measurement noise 100 times lower than the quantum-projection limit using entangled atoms, *Nature*. **advance online publication**, – (Jan., 2016). ISSN 1476-4687. URL <http://dx.doi.org/10.1038/nature16176>.
- [44] H. Metcalf and P. van der Straten, *Laser Cooling and Trapping*. Graduate Texts in Contemporary Physics, Springer New York (2001). ISBN 9780387987286. URL <https://books.google.fr/books?id=i-40VaXqrj0C>.
- [45] J. Le Gouet, P. Cheinet, J. Kim, D. Holleville, A. Clairon, A. Landragin, and F. P. D. Santos, Influence of lasers propagation delay on the sensitivity of atom interferometers, *Eur. Phys. J. D*. **44**, 419–425 (2007).
- [46] J. Harms, B. J. J. Slagmolen, R. X. Adhikari, M. C. Miller, M. Evans, Y. Chen, H. Müller, and M. Ando, Low-frequency terrestrial gravitational-wave detectors, *Phys. Rev. D*. **88**, 122003 (Dec, 2013). doi: 10.1103/PhysRevD.88.122003. URL <http://link.aps.org/doi/10.1103/PhysRevD.88.122003>.
- [47] W. Chaibi, R. Geiger, B. Canuel, A. Bertoldi, A. Landragin, and P. Bouyer, Low frequency gravitational wave detection with ground-based atom interferometer arrays, *Phys. Rev. D*. **93**, 021101 (Jan, 2016). doi: 10.1103/PhysRevD.93.021101. URL <http://link.aps.org/doi/10.1103/PhysRevD.93.021101>.
- [48] N. Yu and M. Tinto, Gravitational wave detection with single-laser atom interferometers, *General Relativity and Gravitation*. **43**(7), 1943–1952 (2011).

ISSN 0001-7701.

- [49] P. W. Graham, J. M. Hogan, M. A. Kasevich, and S. Rajendran, New method for gravitational wave detection with atomic sensors, *Phys. Rev. Lett.* **110**, 171102 (Apr, 2013). doi: 10.1103/PhysRevLett.110.171102. URL <http://link.aps.org/doi/10.1103/PhysRevLett.110.171102>.
- [50] P. L. Bender, Comparison of atom interferometry with laser interferometry for gravitational wave observations in space, *Phys. Rev. D.* **89**, 062004 (Mar, 2014). doi: 10.1103/PhysRevD.89.062004. URL <http://link.aps.org/doi/10.1103/PhysRevD.89.062004>.
- [51] T. Mazzoni, X. Zhang, R. Del Aguila, L. Salvi, N. Poli, and G. M. Tino, Large-momentum-transfer bragg interferometer with strontium atoms, *Phys. Rev. A.* **92**, 053619 (Nov, 2015). doi: 10.1103/PhysRevA.92.053619. URL <http://link.aps.org/doi/10.1103/PhysRevA.92.053619>.
- [52] M. Beccaria, M. Bernardini, S. Braccini, C. Bradaschia, A. Bozzi, C. Casciano, G. Cella, A. Ciampa, E. Cuoco, G. Curci, E. D'Ambrosio, V. Dattilo, G. D. Carolis, R. D. Salvo, A. D. Virgilio, A. Delapierre, D. Enard, A. Errico, G. Feng, I. Ferrante, F. Fidecaro, F. Frasconi, A. Gaddi, A. Gennai, G. Genaro, A. Giazotto, P. L. Penna, G. Losurdo, M. Maggiore, S. Mancini, F. Palla, H. B. Pan, F. Paoletti, A. Pasqualetti, R. Passaquieti, D. Passuello, R. Poggiani, P. Popolizio, F. Raffaelli, S. Rapisarda, A. Vicer©, and Z. Zhang, Relevance of newtonian seismic noise for the virgo interferometer sensitivity, *Classical and Quantum Gravity.* **15**(11), 3339– (1998). ISSN 0264-9381. URL <http://stacks.iop.org/0264-9381/15/i=11/a=004>.
- [53] F. Acernese et al, Advanced virgo: a second-generation interferometric gravitational wave detector, *Classical and Quantum Gravity.* **32**(2), 024001 (2015). URL <http://stacks.iop.org/0264-9381/32/i=2/a=024001>.
- [54] The LIGO Scientific Collaboration, Advanced ligo, *Classical and Quantum Gravity.* **32**(7), 074001– (2015). ISSN 0264-9381. URL <http://stacks.iop.org/0264-9381/32/i=7/a=074001>.
- [55] M. Punturo et al, The einstein telescope: a third-generation gravitational wave observatory, *Classical and Quantum Gravity.* **27**(19), 194002 (2010). URL <http://stacks.iop.org/0264-9381/27/i=19/a=194002>.
- [56] P. Amaro-Seoane et al, Low-frequency gravitational-wave science with elisa/ngo, *Classical and Quantum Gravity.* **29**(12), 124016 (2012). URL <http://stacks.iop.org/0264-9381/29/i=12/a=124016>.
- [57] B. Sathyaprakash and B. F. Schutz, Physics, astrophysics and cosmology with gravitational waves, *Living Rev. Relativity.* **12**, 2 (2009). doi: 10.12942/lrr-2009-2. URL <http://relativity.livingreviews.org/Articles/lrr-2009-2/>.
- [58] The MIGA collaboration (2016). MIGA: Exploring gravity with large scale atom interferometry, in preparation (New Journal of Physics).
- [59] S. M. Dickerson, J. M. Hogan, A. Sugarbaker, D. M. S. Johnson, and M. A. Kasevich, Multiaxis inertial sensing with long-time point source atom interferometry, *Phys. Rev. Lett.* **111**, 083001 (Aug, 2013). doi: 10.1103/PhysRevLett.111.083001. URL <http://link.aps.org/doi/10.1103/PhysRevLett.111.083001>.

- A. Sugarbaker, J. M. Hogan, and M. A. Kasevich, Quantum superposition at the half-metre scale, *Nature*. **528**(7583), 530–533 (Dec., 2015). ISSN 0028-0836. URL <http://dx.doi.org/10.1038/nature16155>.
- [70] N. Robins, P. Altin, J. Debs, and J. Close, Atom lasers: Production, properties and prospects for precision inertial measurement, *Physics Reports*. **529**(3), 265–296 (Aug., 2013). ISSN 0370-1573. URL <http://www.sciencedirect.com/science/article/pii/S037015731300118X>.
- [71] V. Bolpasi, N. K. Efremidis, M. J. Morrissey, P. C. Condylis, D. Sahagun, M. Baker, and W. von Klitzing, An ultra-bright atom laser, *New Journal of Physics*. **16**(3), 033036– (2014). ISSN 1367-2630. URL <http://stacks.iop.org/1367-2630/16/i=3/a=033036>.
- [72] M. G. Raizen, D. Budker, S. M. Rochester, J. Narevicius, and E. Narevicius, Magneto-optical cooling of atoms, *Opt. Lett.* **39**(15), 4502–4505 (2014). URL <http://ol.osa.org/abstract.cfm?URI=ol-39-15-4502>.
- [73] M. Meunier, I. Dutta, R. Geiger, C. Guerlin, C. L. Garrido Alzar, and A. Landragin, Stability enhancement by joint phase measurements in a single cold atomic fountain, *Phys. Rev. A*. **90**, 063633 (Dec, 2014). doi: 10.1103/PhysRevA.90.063633. URL <http://link.aps.org/doi/10.1103/PhysRevA.90.063633>.
- [74] I. Dutta, D. Savoie, B. Fang, C. Garrido Alzar, R. Geiger, and A. Landragin, Continuous cold atom inertial sensor with 1 nrad/s rotation stability, *Phys. Rev. Lett.* (2016). URL <http://journals.aps.org/prl/abstract/10.1103/PhysRevLett.116.183003>.